

Article

Performance of TRMM Product in Quantifying Frequency and Intensity of Precipitation during Daytime and Nighttime across China

Yun Li ¹, Bin Guo ², Kaicun Wang ¹, Guocan Wu ^{1,*} and Chunming Shi ¹

¹ State Key Laboratory of Earth Surface Processes and Resource Ecology, College of Global Change and Earth System Science, Beijing Normal University, Beijing 100875, China; 201921490009@mail.bnu.edu.cn (Y.L.); kcwang@bnu.edu.cn (K.W.); chunming.shi@bnu.edu.cn (C.S.)

² College of Geomatics, Shandong University of Science and Technology, Qingdao 266590, China; guobin07@mailsucas.ac.cn

* Correspondence: gcwu@bnu.edu.cn; Tel.: +86-10-5880-3143; Fax: +86-10-5880-0059

Received: 13 January 2020; Accepted: 20 February 2020; Published: 23 February 2020



Abstract: The Tropical Rainfall Measurement Mission (TRMM) satellite is the first to be designed to measure precipitation, and its precipitation products have been assessed in a variety of ways. Data for its post-real-time level 2 product (3B42) performed well in terms of the precipitation amount at the monthly scale because they were corrected by a precipitation dataset that was gauged every month. However, the performance of this dataset in terms of precipitation frequency and intensity is still not ideal. To this end, TRMM 3B42 products were evaluated using precipitation data from 747 meteorological stations over mainland China in this study. The Pearson's correlation coefficient (CC), relative bias (RB), and relative error (RE) were used to assess the capability of TRMM products in terms of estimating the frequency, intensity, and amount of precipitation for different categories of precipitation during nighttime and daytime in a multiscale analysis (including interannual variation, seasonal cycles, and spatial distribution). Our results showed the following: (1) The 3B42 products reproduced interannual trends of the frequency and amount of precipitation (except for trace precipitation) with an average correlation coefficient of 0.84. (2) 3B42 performed well at calculating the annual and monthly precipitation amount, but performed poorly for frequency and even worse for intensity. The biases in these two properties canceled out, however, which led to a better estimate of the amount. (3) 3B42 represented the distribution of the subdaily amount of precipitation over a majority of the regions in the east, but did not perform well on the Tibetan Plateau or in northwest China. The performance of 3B42, as detailed in this study, can serve as valuable guidance to data users and algorithm developers.

Keywords: TRMM 3B42V7; spatial-temporal variations; nighttime-daytime contrast; precipitation frequency; precipitation intensity; precipitation amount

1. Introduction

Precipitation is among the most important meteorological and climatic variables [1]. It features complex temporal and spatial variations, and is a key factor in regional weather changes and the formation of the global climate [2,3]. Short and intense precipitation can cause floods [4], but droughts occur if it does not rain for a long time [5]. Therefore, obtaining accurate precipitation data to understand the relevant mechanism is important for reducing its negative impacts on the environment and society [5,6].

Current methods for measuring precipitation include ground observations from rain gauges and radars, and estimates inferred from satellite sensors [7,8]. Rain gauge observations constitute the

most primitive and direct method for measuring precipitation, but are often restricted by the number and uneven spatial distribution of meteorological stations [9], especially in developing countries and areas with complex terrains [10]. Weather radar can provide high-resolution precipitation with continuous spatial coverage [11], but has limitations in terms of the transmission of electronic signals, barriers posed by mountains, and cold weather [7,12,13]. Satellite precipitation products have received increasing research interest owing to their wide range of observations, high spatiotemporal resolution, free availability, and real-time access to data [14,15].

Supported by these satellite and remote sensing technologies, many research institutions and government organizations have developed a series of rainfall datasets at both the regional and the global scales [2], such as the Tropical Rainfall Measurement Mission (TRMM) [16,17], the Climate Precipitation Center Morphing Method (CMORPH) [18], the Precipitation Estimation from Remotely Sensed Information using Artificial Neural Network (PERSIANN) [19], and the Global Precipitation Measurement (GPM) [20]. These rainfall products have wide coverage and high resolution to compensate for a lack of spatial distribution of the ground stations and satisfy the needs of data-deficient areas. Of the satellite precipitation products, the TRMM product is considered among the most reliable, and is widely used [11,21–23].

With the continual release of satellite data, research is underway on verifying the accuracy of TRMM satellite data, especially its post-real-time version 7 level 2 product (3B42V7) [17,24]. Varikoden et al. analyzed the temporal and spatial distributions of the intensity of precipitation in the Malay Peninsula [25]. Pombo and Oliveira used 3B42 products to predict extreme precipitation in Angola, and achieved good results [26]. Nastos et al. analyzed the annual and seasonal spatial distributions of differences between the results of TRMM products and gauge observations over Greece [27]. Related researches have also been conducted in the La Plata Basin [28], Amazon Basin [29], Saudi Arabia [30,31], India [32], Iran [33], China [14,34–36], and the United States [37–39].

Because the research version data of the 3B42 have been corrected by a monthly ground precipitation dataset, it is clear that the monthly amount of precipitation is representative, as has been confirmed by several studies [17,40,41]. However, other important properties of precipitation, such as the frequency and intensity, also needed to be evaluated. Past studies have also shown that the 3B42 data can adequately capture the spatial variation in annual and seasonal precipitation [10]. Nevertheless, it tends to overestimate trace precipitation and underestimate torrential precipitation at the daily scale owing to inadequate detection capability [10,42]. Therefore, whether 3B42 products and ground data can obtain the same effect for different categories of precipitation needs to be determined.

Moreover, the mechanisms of precipitation are different during the daytime and nighttime due to the diurnal variation in solar radiation, relative humidity, and the type of clouds with dominant precipitation [43–45]. As the TRMM satellite calculates precipitation from the scattering of ice crystals in clouds, the differences in the types of precipitation clouds can significantly affect the quality of satellite data [16]. Consequently, it is important to check the variation in precipitation reproduced by the 3B42 product during the daytime and nighttime, which is also important for understanding the physical mechanism of precipitation.

This study makes assesses performance of 3B42 data in terms of quantifying the frequency and intensity of precipitation during daytime and nighttime through station observations. Subdaily precipitation data were collected from approximately 800 meteorological stations in mainland China from 1998 to 2017. The interannual variation and seasonal cycle of subdaily precipitation are analyzed and compared between the 3B42 data and station observations. The spatial distributions of relative biases between data from the satellite and stations at the subdaily scale are examined. The correlation coefficient (CC), relative bias (RB) and relative error (RE) are used to assess the capability of the TRMM 3B42 to simulate nighttime and daytime precipitation at multiple levels (the frequency, intensity, and amount of precipitation) in different categories ranging from a trace to a large amount of precipitation.

2. Study Area and Data

2.1. Study Area

The study area covered most of China, ranging across 75°E–133°E longitude and 16°N–50°N latitude. The vast territory, location near the Pacific Ocean, and descending three-terrace topography create large differences in climate among the regions of the country. A topographical map of the study area with a diagrammatic sketch of the main mountains is shown in Figure 1.

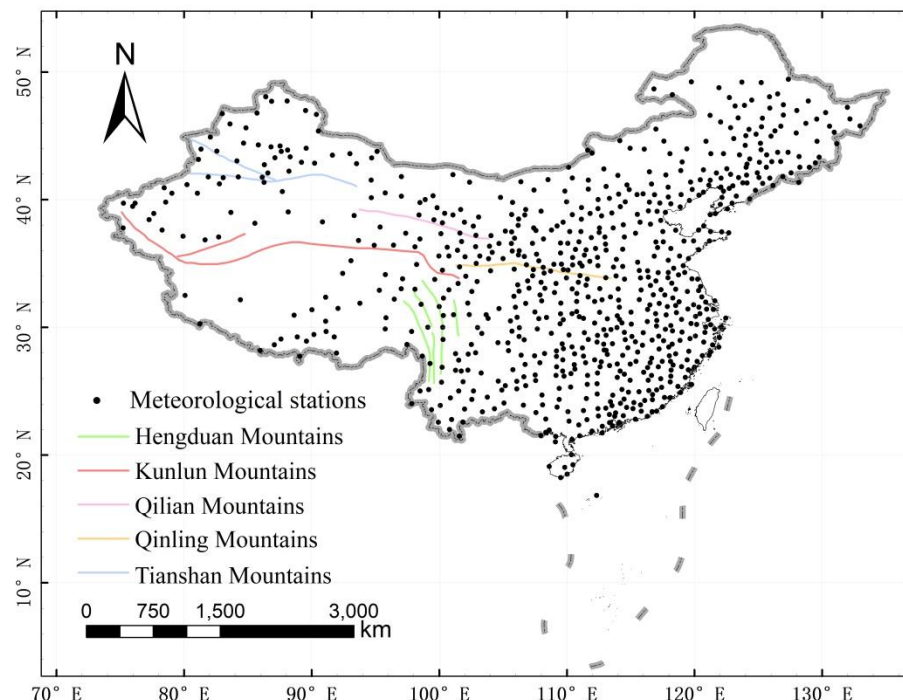


Figure 1. The diagrammatic sketch of the main mountains and distribution of meteorological stations in the study area. The datasets were obtained from China Meteorological Administration (CMA; <http://data.cma.cn/en/>).

Affected by monsoons from the Pacific Ocean and Indian Ocean, the country is warm and humid in the summer, especially in the eastern regions. In the winter, cold and dry winds from the interior of Asia lead to lower precipitation and temperatures in China, especially in the northern regions. Owing to the wide-ranging influence of winter and summer monsoons, China is hot and rainy in the same period. In general, there is much more precipitation in the summer than in the winter, with significant changes in interannual variation. The spatial distribution of precipitation is also uneven in China, and annual precipitation gradually decreases from the southeast to the northwest.

2.2. Satellite-Based Precipitation Products

The Tropical Rainfall Measuring Mission (TRMM) is a joint mission between the National Aeronautics and Space Administration (NASA) of the United States and the National Space Development Agency (NASDA) of Japan [16]. It was launched in Japan on 27 November 1997, and carried a TRMM microwave imager (TMI), a precipitation radar (PR), visible and infrared scanner (VIRS), clouds and earth radiant energy system (CERES), and a lightning image sensor (LIS) [16,46]. The TMI, PR, and VIRS are basic precipitation-measuring instruments for TRMM satellites. The TRMM observatory was designed to observe rainfall to provide accurate global tropical precipitation estimates [16,46,47].

The TRMM satellite consists of two products, a near-real-time version (3B42RT) and a gauge-adjusted post-real-time research version (3B42). The former covers the global latitude belt from

60°S to 60°N, providing quick but less accurate estimates suitable for real-time observation. The latter covers the range from 50°S to 50°N, providing more accurate estimates that are more suitable for research [48]. To reduce the random error in comparison with precipitation products of version 6, both have updated to version 7 using the latest correction algorithm to improve accuracy [34,41,48–50]. Compared with 3B42RT data, the formation of the precipitation products of 3B42 is complex for many reasons. First, the precipitation data at the monthly scale are obtained from 3B42RT products. Second, monthly scale-related data are recalibrated using the monthly dataset of the Global Precipitation Climatology Centre (GPCC). Third, the recalibrated monthly data are rescaled to a 3-h resolution to reproduce the 3B42 research version. Details of the algorithm can be found in studies by Iguchi et al. [51] and Dinku and Anagnostou [52].

The TRMM data used in this study were from the post-real-time TRMM satellite version 7 level 2 product (3B42V7), from the National Aeronautics and Space Administration (NASA; https://disc.gsfc.nasa.gov/datasets/TRMM_3B42_7/summary), with a spatial resolution of $0.25^\circ \times 0.25^\circ$ and a 3-h time step (0000, 0300, ..., 2100 UTC). It was evaluated using gauge-based precipitation observations in mainland China from 1 January 1998 to 31 December 2017.

2.3. Gauge-Based Precipitation Observations

The meteorological precipitation observations are recorded in Beijing Time (short for BT hereafter). The daytime (08:00–20:00 BT) and nighttime (20:00–08:00 BT) data, with a full time series of subdaily precipitation data from 800 meteorological stations in mainland China from 1 January 1998 to 31 December 2017, were obtained from the China Meteorological Administration (CMA; <http://data.cma.cn/en/>). This dataset has undergone a series of strict quality control measures and homogenization, including the climate limit value or allowable value check, internal consistency checks, and spatiotemporal consistency tests [53].

To ensure the integrity of data, the dataset was screened and inspected in this study. By referring to the scope of satellite observations (50°S – 50°N), meteorological stations in the northernmost parts of China, above 50° N in Heilongjiang Province and the Inner Mongolia Autonomous Region, were excluded. Station observations that had missing values for an entire month in any of the 240 months during the research period (1998–2017) were discarded. Finally, the missing subdaily data of these stations for each month were calculated, and defects due to instrument errors and bad weather were marked. Because each station had two records per day (08:00–20:00 BT and 20:00–08:00 BT), data from stations with less than 15% of data missing for both time periods were retained. Following these procedures, a total of 747 stations met the requirements and were used in this study. They were denser in the east than in the west, especially in the northwestern and the Tibetan Plateau. The distribution of the stations is shown in Figure 1.

3. Methodology

3.1. Data Preprocessing

To evaluate the precipitation data from the meteorological stations and grids of the remote sensing products, the general approach used was to generate data from the former to the latter. However, such spatial interpolation usually incurred additional errors, especially in western China, due to the sparseness of stations [21,54]. Alternatively, this study directly compared meteorological observations with those of the satellite grid data centers where the meteorological stations were located. Therefore, the 747 meteorological stations corresponded to 747 grid points, whereas grids that did not contain any meteorological stations were excluded.

To eliminate errors between satellite products and station observations caused by different time zones, the time at which the satellite data were captured were transformed from UTC to Beijing time. That is, the nighttime represented 12:00–24:00 UTC or 20:00–08:00 BT, and the daytime represented 12:00–24:00 UTC or 08:00–20:00 BT.

The satellite precipitation dataset had a 3-hour temporal resolution, and was stored in the date-hour format. For example, 3B42.19980101.12.7 is the data recorded at 12:00 UTC, which represents the average amount of precipitation (in mm/h) over 3 h from 10:30 UTC to 13:30 UTC on January 1, 1998. To coordinate this with Beijing time during the day, we assigned a weight of 0.5 to data recorded at 00:00 UTC and 12:00 UTC, and a weight of 1 to those recorded at 03:00, 06:00, and 09:00 UTC. Subsequently, these weighted data were summed and multiplied by a factor of 3 to obtain the amount of precipitation, as recorded by 3B42V7 during the daytime. Similarly, data for 12:00 UTC and 24:00 UTC were assigned a weight of 0.5 while those recorded at 15:00, 18:00, and 21:00 UTC were assigned a weight of 1. Then, these weighted data were summed and multiplied by a factor of 3 to obtain the amount of precipitation during the night.

3.2. Precipitation Classification and Properties

In this study, a precipitation event is defined as an instance of precipitation greater than or equal to 0.1 mm within 12 h during the daytime or nighttime. According to the amount of precipitation, each precipitation event is classified into the following four categories of intensity: trace ($0.1 \leq P < 1 \text{ mm (12 h)}^{-1}$), small ($1 \leq P < 10 \text{ mm (12 h)}^{-1}$), moderate ($10 \leq P < 25 \text{ mm (12 h)}^{-1}$), and large ($P \geq 25 \text{ mm (12 h)}^{-1}$). The similar classification has been used in many related studies [55–57].

Three properties of precipitation, i.e., its frequency, intensity, and amount, were analyzed in this study. The precipitation amount in each category was the cumulative precipitation of all precipitation events within it. The precipitation frequency was the number of days with precipitation in a given category. The precipitation intensity for each category was the ratio of its precipitation amount to the duration hours. Similar interpretations of the frequency, intensity, and amount of precipitation have been used in previous research [58].

3.3. Trend Calculation and Evaluation Indices

Trends of the frequency, intensity, and amount of precipitation were calculated based on the following regression equation:

$$Pr(t) = at + b + \varepsilon, \quad (1)$$

where Pr refers to the frequency, intensity, or amount of precipitation, t is time, a is the corresponding trend, b is the constant term, and ε refers to error in the equation. Regression analysis is used to describe the trends of satellite estimates and station observations at the interannual scale. The P value was used to indicate the level of significance.

According to the evaluation indicators of meteorological satellite products and assessment reports, the Pearson's correlation coefficient (CC), relative bias (RB), and relative error (RE) were used to assess consistency between the satellite products and station observations in this study. The formulae for these indicators are as follows:

$$CC = \frac{\sum_{i=1}^n (T_i - \bar{T})(G_i - \bar{G})}{\sqrt{\sum_{i=1}^n (T_i - \bar{T})^2} \sqrt{\sum_{i=1}^n (G_i - \bar{G})^2}}, \quad (2)$$

$$RB = \frac{\sum_{i=1}^n (T_i - G_i)}{\sum_{i=1}^n G_i} \times 100\%, \quad (3)$$

and

$$RE = \frac{\sum_{i=1}^n |T_i - G_i|}{\sum_{i=1}^n G_i} \times 100\%, \quad (4)$$

where T_i and G_i refer to the TRMM data and the gauge data, respectively. $\bar{T} = \frac{1}{n} \sum_{i=1}^n T_i$ and $\bar{G} = \frac{1}{n} \sum_{i=1}^n G_i$ are the mean values, and n is the number of precipitation events. The value of CC ranged from -1 to 1 , indicating the fitness of the temporal variation between satellite estimates and station observations. $CC > 0$ represents a positive correlation and $CC < 0$ represents a negative correlation. Furthermore, $0 \leq |CC| < 0.2$ represents extremely weak or irrelevant correlation, $0.2 \leq |CC| < 0.4$ represents weak correlation, $0.4 \leq |CC| < 0.6$ means moderate correlation, $0.6 \leq |CC| < 0.8$ means strong correlation, and $0.8 \leq |CC| \leq 1.0$ denotes extremely strong correlation. RB denotes the estimated effect of the satellite products on station observations [59]. $RB > 0$ implies that the satellite product has overestimated precipitation and $RB < 0$ means that it has underestimated precipitation. If RB is close to zero, the TRMM data are closer to the gauge data on average. RE can give an estimate of the accuracy of the satellite measurement from the point of volatility. Basically, the satellite data have less volatility when there is a smaller RE value.

4. Results

4.1. Interannual Variation in Subdaily Precipitation Properties

Figure 2 shows the interannual variations and linear trends of the precipitation frequencies of the TRMM 3B42 and gauge data during nighttime and daytime for the categories of trace, small, moderate, and large amounts of precipitation in the period 1998–2017. In general, TRMM 3B42 products roughly reproduced the interannual trends of the precipitation frequencies over mainland China in the last two decades, excluding the frequency of trace amounts of rain (Figure 2a₁,b₁). Specifically, TRMM had the strongest correlation with gauge data in terms of moderate and large amounts of rain ($CC > 0.9$), a moderate correlation for small amounts of rain ($CC = 0.562$ and $CC = 0.470$ for nighttime and daytime, respectively), and an insignificant correlation for trace amounts of rain.

The frequencies of trace amounts of rain were significantly underestimated by the TRMM 3B42, by 31.82% during the nighttime and 26.61% during the daytime. For the frequencies of small amounts of rain, there were diurnal differences in the estimates of the satellite. At night, the TRMM 3B42 underestimated the frequency of small amounts of rain ($RB = -3.48\%$), and overestimated it in the daytime ($RB = 4.6\%$). It only slightly underestimated moderate amounts of rain ($RB = -0.17\%$), indicating good performance for moderate precipitation frequency during the nighttime. During the daytime, for moderate and large amounts of rain, the TRMM 3B42 tended to slightly overestimate the frequency ($RB = 10\%$). Because the frequency of mild precipitation (trace or small amounts of rain) contributes the most to the total precipitation frequency, the correlation of TRMM and gauge data in terms of the total precipitation frequency was weak, and the satellite underestimated the total precipitation frequency.

According to station observations, the frequency of precipitation as trace amounts of rain over the past two decades fluctuated slightly. However, as detected by satellites, it decreased at a rate of 5.8 d/10 a during the nighttime and 4.9 d/10 a during the daytime, which were significant values at the 0.01 level based on the significance test. For small amounts of rain, the precipitation frequency from the stations was relatively stable, with a slight oscillation around 35 days, but the satellite estimates recorded a significant difference between the daytime and nighttime. Precipitation frequency, as recorded by the satellite, decreased at a rate of 1.5 d/10 a during the nighttime at a significance level of 0.05. On the contrary, it gradually increased at 0.6 d/10 a during the daytime, but without any significance.

The satellite products recorded a strong correlation at stations with moderate and large amounts of rain, and their trends of increase were similar to those obtained using station observations.

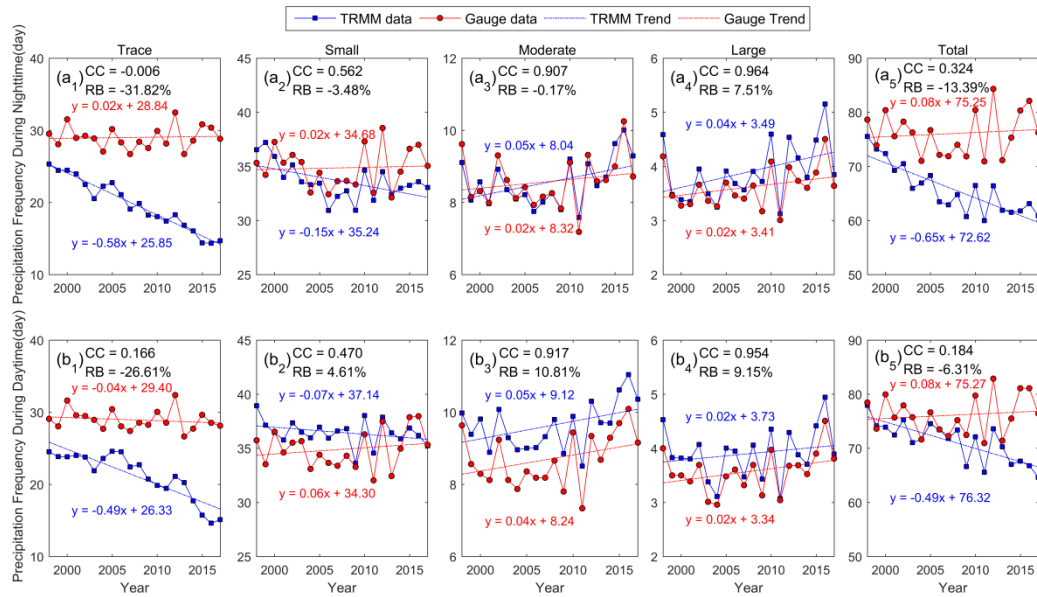


Figure 2. Interannual variations and linear trends of precipitation frequencies from TRMM 3B42 data and gauge data during the (a) nighttime and (b) daytime for different categories of intensity from 1998 to 2017 over mainland China. From left to right are days with a trace amount of rain ($(0.1 \leq P < 1 \text{ mm (12 h)}^{-1})$), a small amount of rain ($1 \leq P < 10 \text{ mm (12 h)}^{-1}$), a moderate amount of rain ($10 \leq P < 25 \text{ mm (12 h)}^{-1}$), a large amount of rain ($P \geq 25 \text{ mm (12 h)}^{-1}$), and the total precipitation ($P \geq 0.1 \text{ mm (12 h)}^{-1}$). The y-axis scales are different for different precipitation categories.

Therefore, in terms of mild precipitation (trace and small amounts of rain), the TRMM 3B42 had considerable deficiencies in reproducing the trend of the interannual precipitation frequency. Moreover, the satellite tended to slightly overestimate the frequency and the trend of moderate and large amounts of rains (intensity higher than $10 \text{ mm (12 h)}^{-1}$), and to significantly underestimate those of other categories of rain (intensity lower than $10 \text{ mm (12 h)}^{-1}$), which is consistent with the results for the southern Tibetan Plateau in past research [60].

Figure 3 shows that the intensities of all four precipitation categories and the total precipitation intensity were overestimated by the TRMM 3B42, with the largest overestimation in the intensity of trace amounts of rain (Figure 3a₁, b₁), whereas it heavily underestimated the frequency of trace amounts of rain. For small, moderate, and large amounts of rain, the TRMM 3B42 slightly overestimated the values, and their corresponding *RB* values were smaller than 3%, indicating that the precipitation intensity based on satellite data was close to the station observations. Due to the overestimation for each category of precipitation, the total precipitation intensity was overestimated by 18.43% and 16.96% during the nighttime and daytime, respectively. Although the satellite overestimated the intensity of trace amounts of rain significantly during the daytime, the TRMM and gauge data were strongly correlated ($CC = 0.817$). This formed a strong contrast with the results for the nighttime ($CC = -0.09$), which indicated significant uncertainty due to system error in the assessment of the intensity of precipitation as a trace amount of rain by the satellite, especially during the nighttime.

In addition to overestimating the precipitation intensity, the satellite data also exhibited a trend of increase, except in the case of a large amount of rain. The increased trends were especially significant for trace, small, and moderate amounts rain at night, all of which passed the significance test at a level of 0.01. This caused the total precipitation intensity (based on satellite data), which passed the test with a significance of 0.05, to also increase annually.

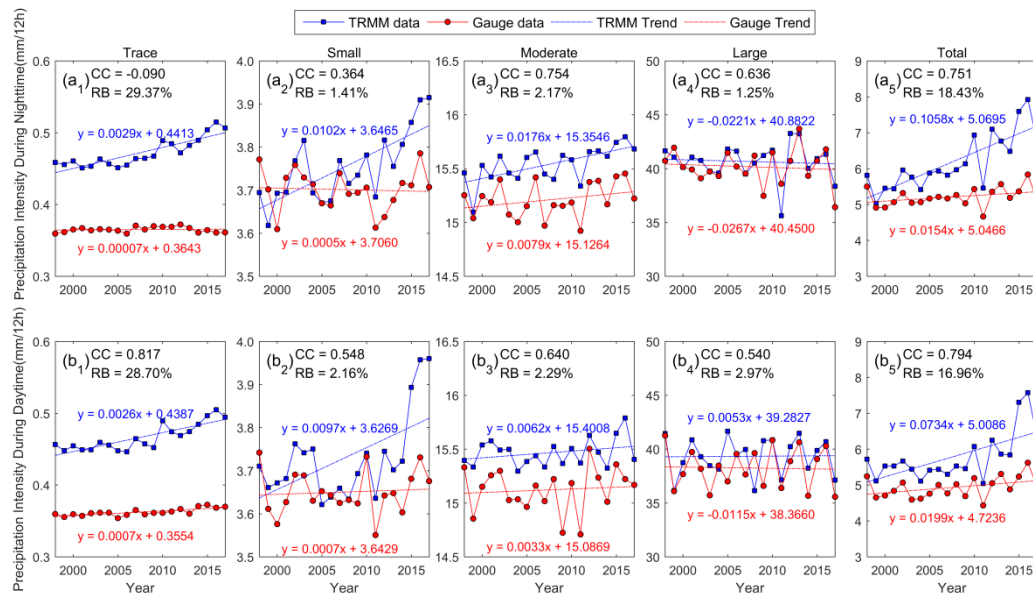


Figure 3. As in Figure 2, but for the intensity of precipitation. The *y*-axis scales are different for different precipitation categories.

Compared with the frequency and intensity of precipitation, the correlation of TRMM and gauge data was the best in terms of the amount of precipitation (Figure 4). Its performance in calculating trace amounts of rain was still poor ($CC < 0.1$), in that they were significantly underestimated. The precipitation amount recorded by satellite data decreased at a rate of 2.2 mm/10 a (nighttime) and 1.8 mm/10 a (daytime), and passed the significance test of 0.01. There were diurnal differences in the assessment of small amounts of rain. The satellite data tended to underestimate the amount during the nighttime but overestimated it in the daytime. It also overestimated moderate and large amounts of rain, but not by much. The average correlation coefficient of the four categories of precipitation intensity was 0.65 and that of total precipitation was above 0.97, showing a strong correlation. The above showed that performance in terms of precipitation amount was more similar for frequency than for intensity.

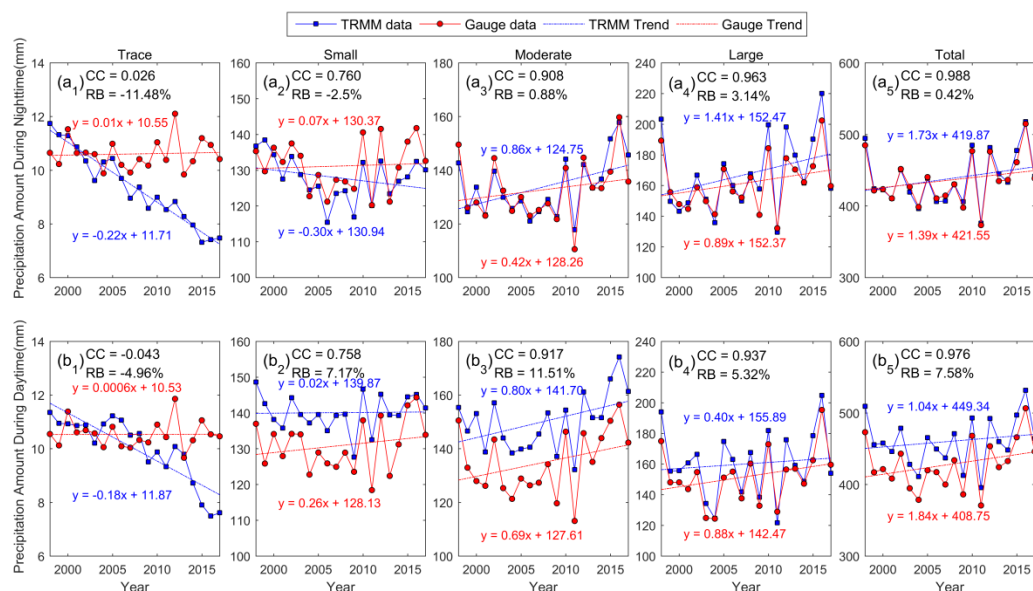


Figure 4. As in Figure 2, but for the amount of precipitation. The *y*-axis scales are different for different precipitation categories.

The TRMM and gauge data showed the best correlation in terms of the total precipitation amount during the nighttime ($CC = 0.988$) due to the underestimation of trace and small amounts of rain being offset by the overestimation of moderate and large amounts of rain. During the daytime, the satellite data overestimated the total precipitation amount by 7.58%, indicating that the underestimation of trace amounts of rain and the overestimation of other types of rain were not completely offset. This also indicated that the satellite data had poorer simulation capability during the day than at night.

4.2. Properties of Seasonal Cycle of Subdaily Precipitation

Figures 5–7 show the multiyear average seasonal variation in the frequency, intensity, and amount of precipitation for trace, small, moderate, and large amounts of precipitation during the nighttime and daytime over China. In general, the TRMM 3B42 effectively reproduced the seasonal shape of the frequency and amount of precipitation during the nighttime and daytime ($CC > 0.88$). In addition, the satellite products could roughly represent the seasonal shape of small and large amounts of rain, and the total precipitation intensity ($CC > 0.8$). However, the satellite products had slight deficiencies in their ability to simulate the shape of trace and moderate precipitation intensity ($CC < 0.67$).

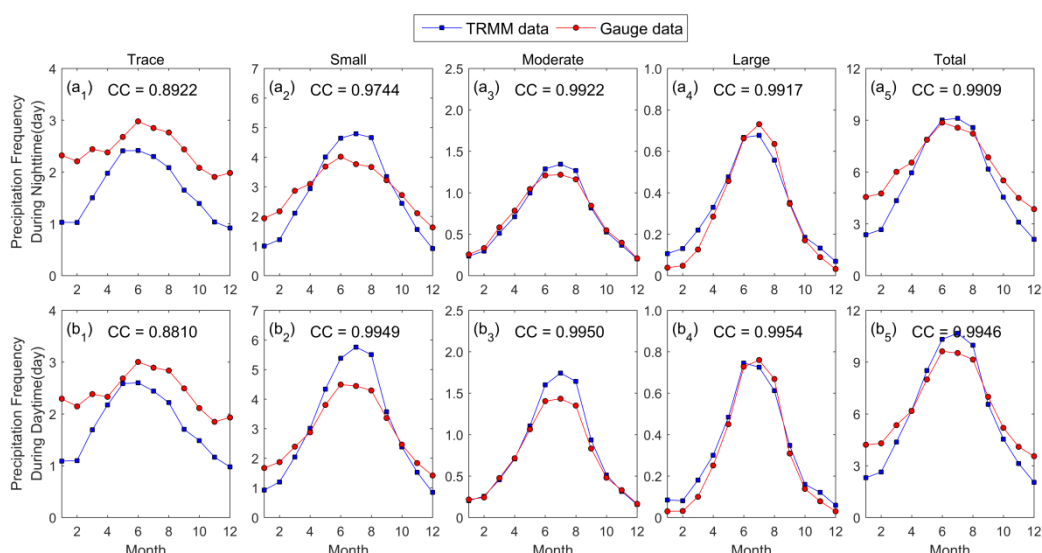


Figure 5. Seasonal cycle of multiyear mean precipitation frequencies from TRMM 3B42 data and gauge data for precipitation frequencies during the (a) nighttime and (b) daytime for various precipitation categories over mainland China. From left to right are days with a trace amount of rain ($(0.1 \leq P < 1 \text{ mm } (12 \text{ h})^{-1})$), a small amount of rain ($1 \leq P < 10 \text{ mm } (12 \text{ h})^{-1}$), a moderate amount of rain ($10 \leq P < 25 \text{ mm } (12 \text{ h})^{-1}$), a large amount of rain ($P \geq 25 \text{ mm } (12 \text{ h})^{-1}$)); and total precipitation ($P \geq 0.1 \text{ mm } (12 \text{ h})^{-1}$). The y-axis scales are different for different precipitation categories.

The frequency of a trace amount of rain was underestimated by the satellite throughout the year during the nighttime ($-55.66\% < RB < -9.90\%$ for each month) and daytime ($-52.50\% < RB < -6.71\%$ for each month), with the largest underestimation in January. However, the intensity of trace amounts of rain was overestimated throughout the year during both the nighttime ($18.46\% < RB < 42.43\%$ for each month) and the daytime ($22.16\% < RB < 37.13\%$ for each month), with the largest overestimation in August. The TRMM and gauge data estimated the amount of mild rain well ($-47.64\% < RB < 21.86\%$ during the daytime and nighttime), with a strong correlation ($CC > 0.9$). Because the biases in the frequency and intensity of precipitation cancel each other out, the calculated amount of precipitation was reasonable.

In addition, in the case of a small amount of rain, the satellite data tended to overestimate the precipitation frequency in May–September (nighttime) and May–October (daytime), but to underestimate the frequency in other months (Figure 5a₂,b₂). Therefore, the seasonal amplitudes of

the precipitation frequencies were exaggerated by the satellite data. This situation also appeared in the seasonal variation of the low precipitation amount (Figure 7a₂,b₂), further indicating that the seasonal cycle of precipitation amount was dominated by the precipitation frequency. Although the precipitation frequency was overestimated or underestimated in different months for the four precipitation categories, there was a prominent convex seasonal shape for the total precipitation frequency. The satellite data tended to overestimate the frequency in rainy months (May–August) and to underestimate it in rainless months (October–March).

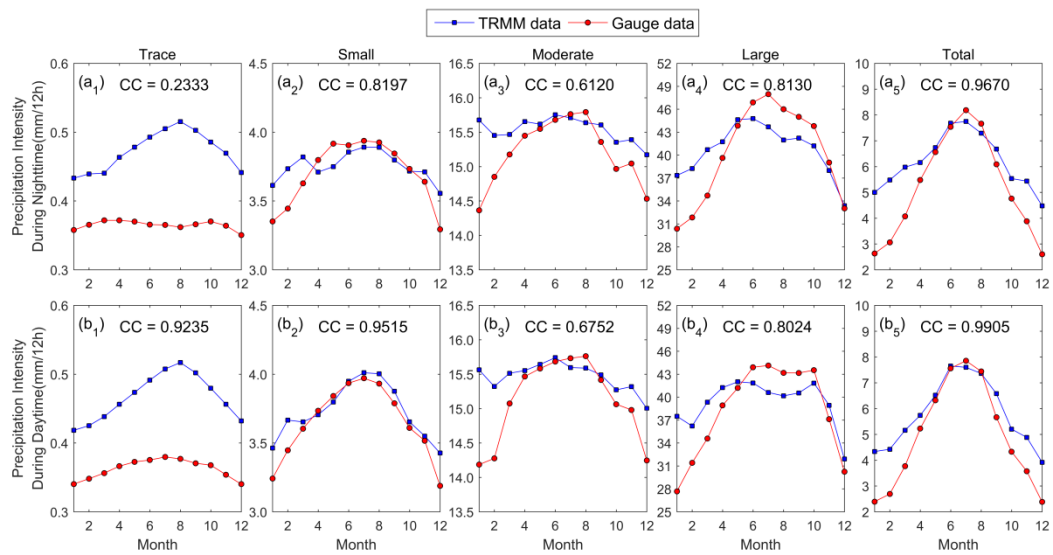


Figure 6. As in Figure 5, but for the intensity of precipitation. The *y*-axis scales are different for different precipitation categories.

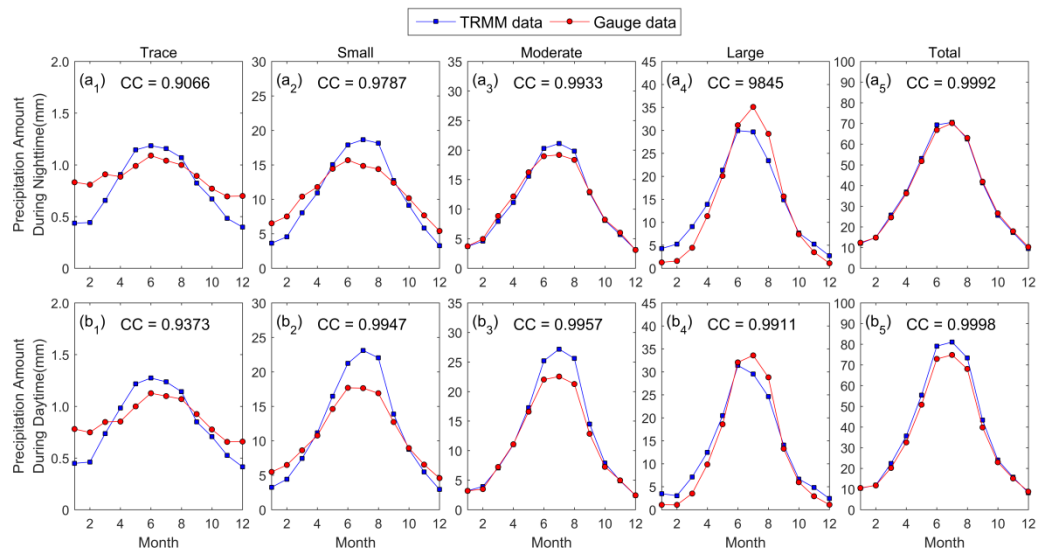


Figure 7. As in Figure 5, but for the amount of precipitation. The *y*-axis scales are different for different precipitation categories.

As a result, the seasonal variations of TRMM data and station observations are not generally consistent with each other for precipitation frequency and intensity. The satellite data underestimated the precipitation intensity from May to August, but overestimated it from September to April. TRMM data had the closest agreement with those from the stations in terms of the total precipitation amount. Therefore, biases in the frequency and intensity of precipitation in each month canceled each other out, which led to the best estimation of the amount of precipitation.

4.3. Properties of Spatial Distribution of Satellite Data and Stations in Subdaily Precipitation

Figures 8–10 show the spatial distribution of the multiyear average relative bias of the frequency, intensity, and amount of precipitation between TRMM 3B42V7 products and station observations for different precipitation categories over mainland China. In general, the spatial distribution of the relative bias in the precipitation frequency was similar to that in precipitation amount, whereas that of the precipitation intensity presented a different situation, especially for trace and small amounts of rain.

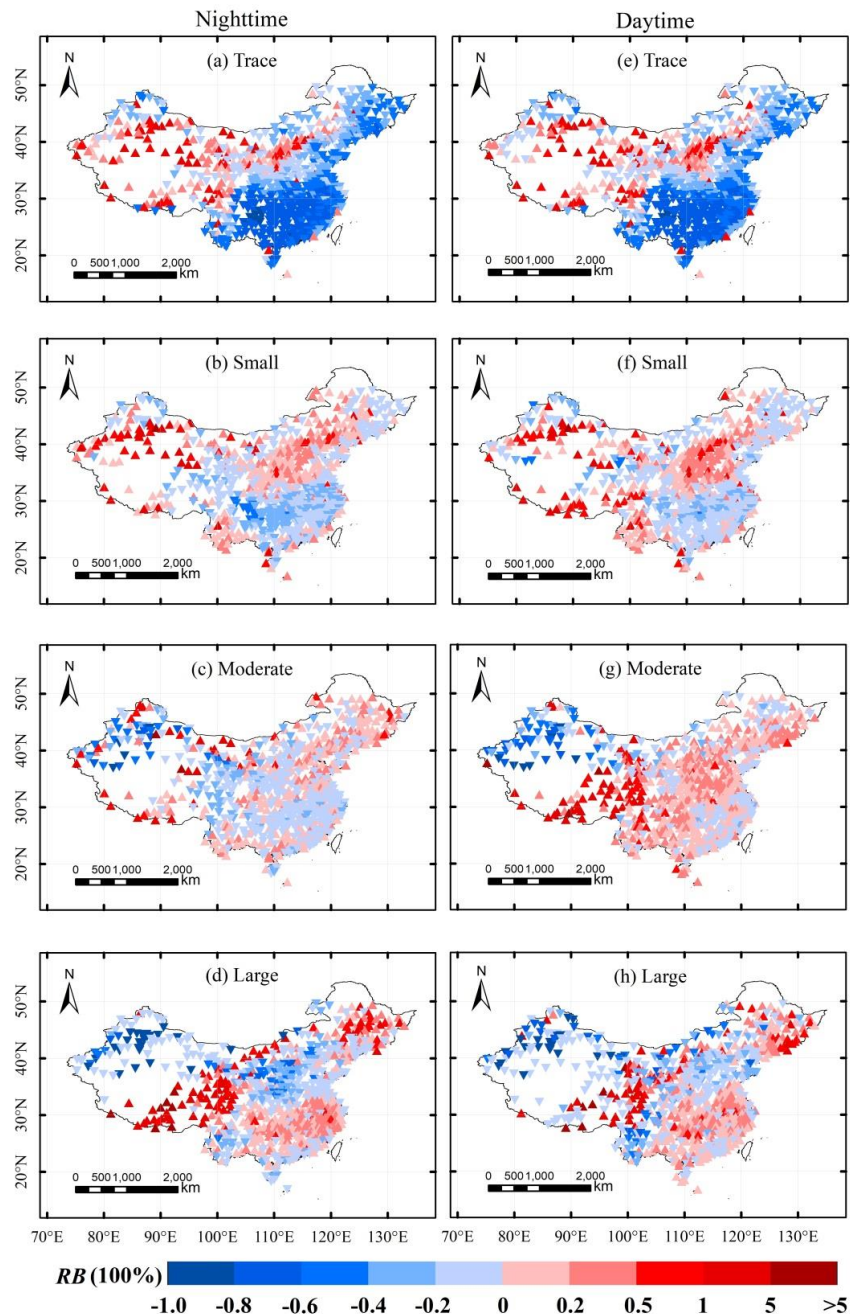


Figure 8. Spatial distribution of relative bias from TRMM 3B42 data and gauge data for precipitation frequencies during (a–d) nighttime and (e–h) daytime for different categories of intensity over mainland China. From top to bottom are days with a trace amount of rain ($(0.1 \leq P < 1 \text{ mm (12 h)}^{-1})$), a small amount of rain ($1 \leq P < 10 \text{ mm (12 h)}^{-1}$), a moderate amount of rain ($10 \leq P < 25 \text{ mm (12 h)}^{-1}$), and a large amount of rain ($P \geq 25 \text{ mm (12 h)}^{-1}$). Regular or inverted triangles represent stations that have a positive or negative relative bias, respectively.

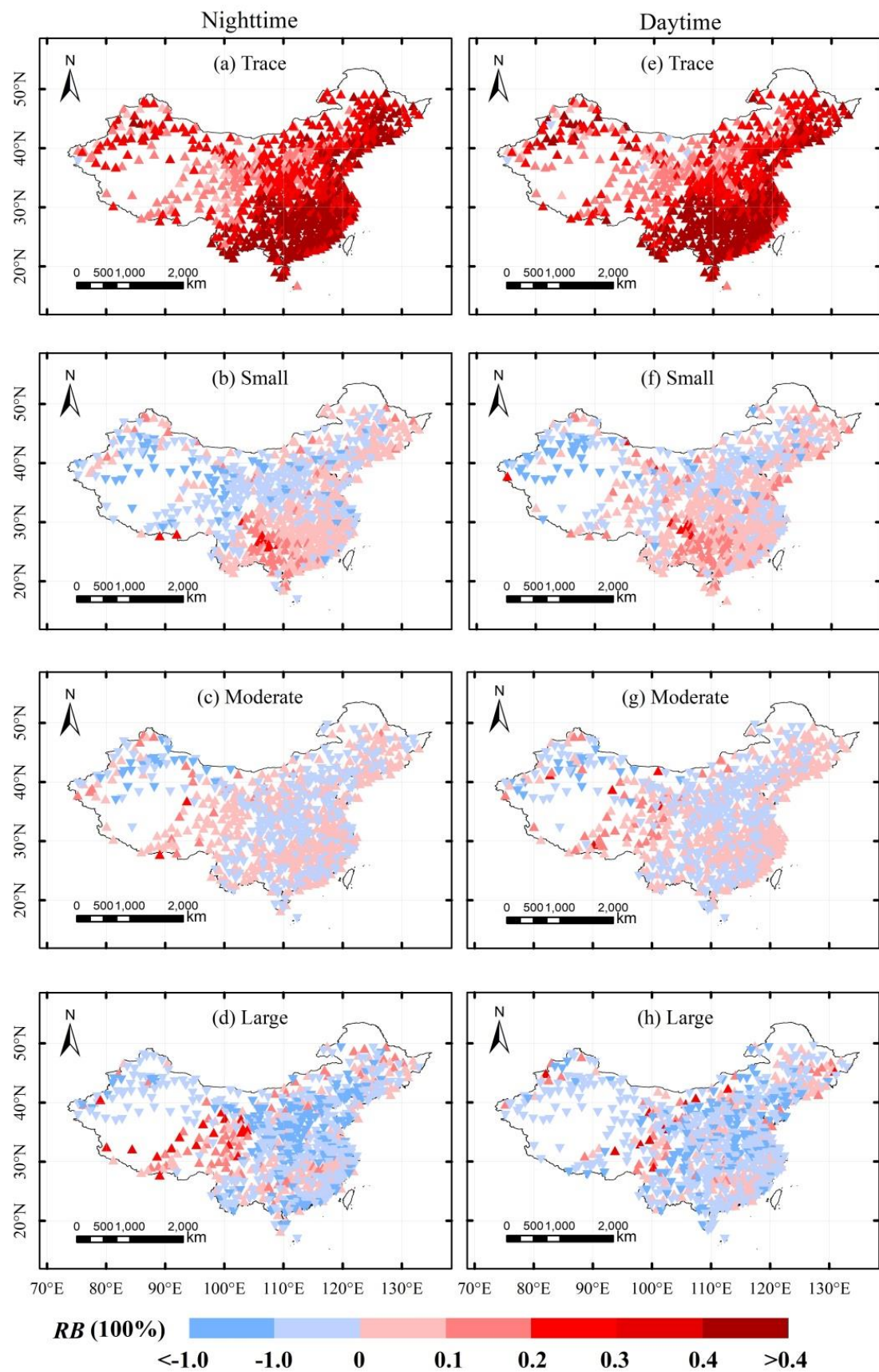


Figure 9. As in Figure 8, but for the intensity of precipitation.

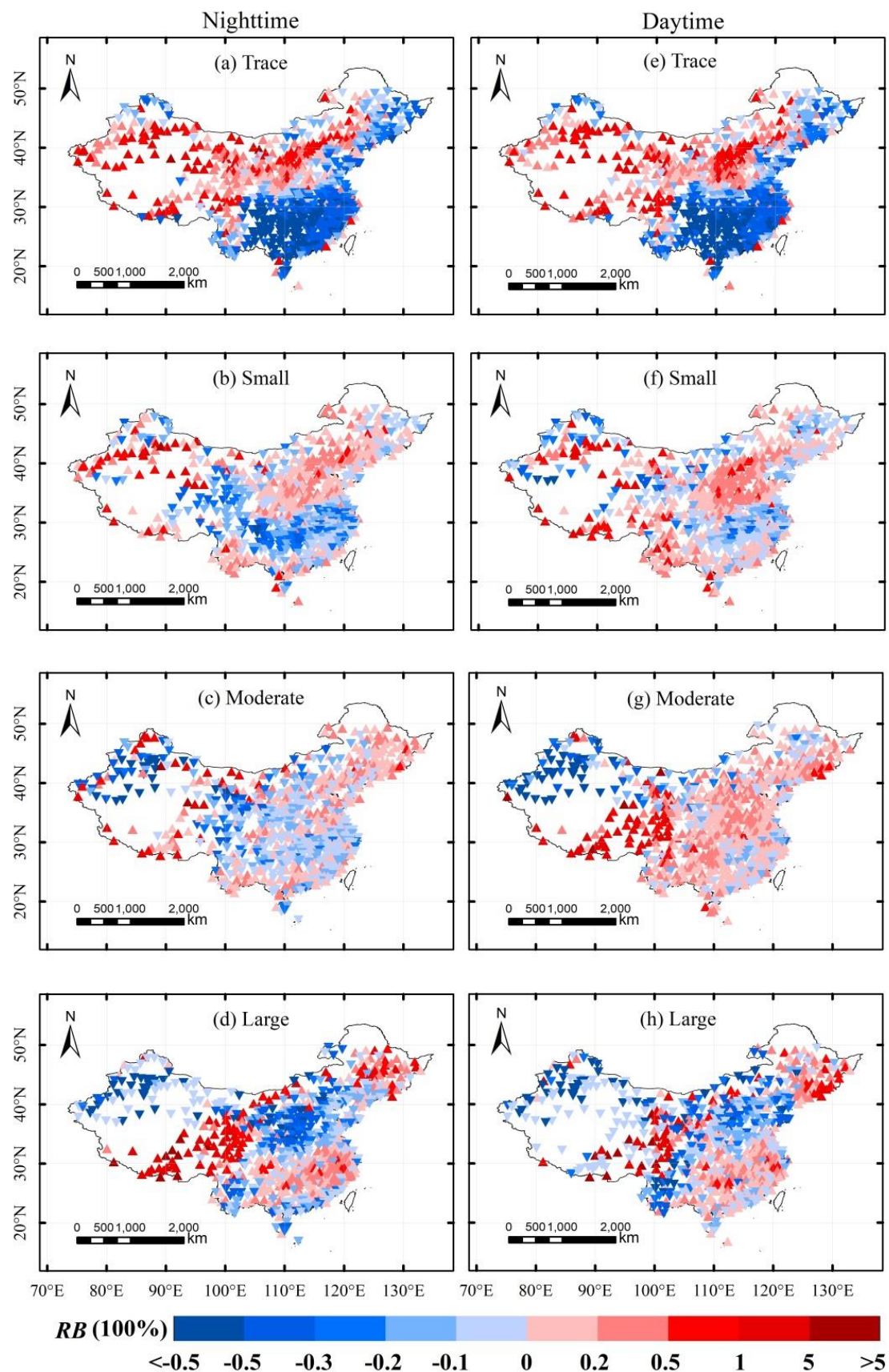


Figure 10. As in Figure 8, but for the amount of precipitation.

Figure 8 shows that for trace amounts of rain, the satellite data underestimated the precipitation frequency for more than 70% of the stations in China, with a value of RB smaller than -85% . However, for other regions, such as the Loess Plateau, the Hengduan Mountains, and western China, the precipitation frequency was heavily overestimated. For small amounts of rain, the range of overestimation by the satellite expanded around the Loess Plateau, but was smaller than 40%. The relative bias in underestimation decreased from -85% for a trace amount of rain to -30% . For a moderate amount of rain, there were differences in the distribution of RB during the nighttime and daytime. Precipitation frequency in most of eastern China was underestimated during the nighttime and overestimated during the daytime, but the relative bias was within 20%, indicating that the satellite had a certain accuracy and reliability for a moderate amount of rain. Heavy rain was overestimated in the south of China and underestimated in northern regions and Yunnan Province, which is contrary to the distribution of the precipitation frequencies in other categories.

For the frequency of precipitation, there was no obvious difference in the patterns of distribution during the nighttime and daytime except in the case of a moderate amount of rain. The satellite data showed a significant north–south gradient for estimating the frequencies of large or trace-small amounts of rain. From trace to large amounts of rain, the range of overestimation of precipitation frequency by the satellite data increased, but the maximum bias was mainly distributed in the Tibetan Plateau.

Figure 9 shows that the satellite data overestimated the precipitation intensity at 99% of the stations over mainland China for small amounts of rain, and the relative bias was larger than 40% for most stations. However, the biases in the precipitation intensity between satellite data and data from stations for the small, moderate, and large amounts of rain were relatively small, and the spatial distribution patterns were not evident.

Figure 10 shows that the pattern of spatial distribution of relative bias between satellite data and data from stations for precipitation amount was similar to that for its frequency. For a trace amount of rain, there was almost no difference between the nighttime and daytime, whereas the spatial distribution of the relative bias was roughly bounded by the Qinling Mountains. Precipitation amount was overestimated by the satellite data in the north of Qinling Mountains, and was underestimated south of Qinling. In western China, the satellite data tended to overestimate the precipitation amount, especially in the Tianshan Mountains, the southern margin of the Tibetan Plateau, and the Qilian–Hengduan Mountains ($RB \geq 200\%$), indicating that the satellite data delivered poor performance in areas with a complex terrain.

Figures 11–13 show the spatial distribution of the multiyear average relative error of the frequency, intensity, and amount of precipitation between TRMM 3B42V7 products and station observations for different precipitation categories over mainland China. Generally, the amplitude of relative error is larger than that of relative bias for each precipitation category, since the positive and negative values can offset the latter statistic. Figure 11 shows that the relative error in the precipitation frequency was larger during the daytime than during the night, while the opposite is the case for the precipitation intensity shown in Figure 12. This leads to relative stability between the nighttime and daytime in terms of the precipitation amounts shown in Figure 13. The lowest amount of rain has the largest relative error among the four precipitation categories (the mean RE is about 50% for precipitation frequency, 40% for precipitation intensity, and 60% for precipitation amount). Spatially, the relative error is larger in northwest China than in other areas, especially for trace and small amounts of rain, indicating that the TRMM 3B42V7 products have large volatility in northwest China.

The maximum underestimation of the precipitation amount by satellite products dropped from 78% for a trace amount of rain to 66% for a small amount of rain, so the degree of underestimation decreased only slightly. The relative bias and relative error between the satellite data and data from stations with a moderate amount of rain were small, similar to the case of interannual variations (Figure 2). This indicated that the satellite data had strong temporal and spatial simulation capabilities for dealing with a moderate amount of rainfall. The spatial distribution of large amounts of rain was significantly different from that of trace and small amounts of rain, and was underestimated in

northwest China. This trend was reversed in east China for a trace amount of rain. It was overestimated in south and northeast China, whereas it was underestimated in north China.

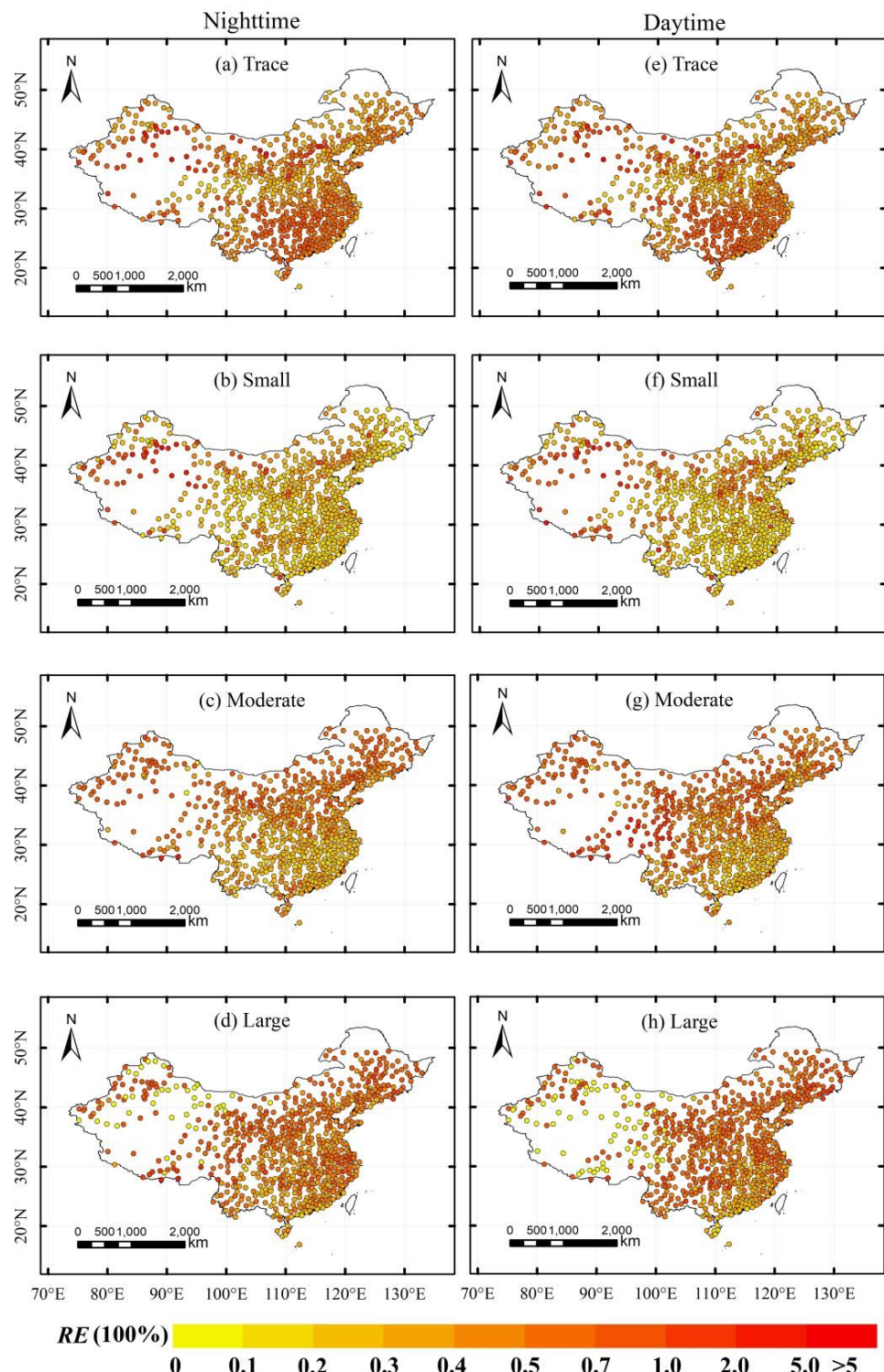


Figure 11. Spatial distribution of relative error from TRMM 3B42 data and gauge data for precipitation frequencies during (a–d) nighttime and (e–h) daytime for different categories of intensity over mainland China. From top to bottom are days with a trace amount of rain ($0.1 \leq P < 1 \text{ mm (12 h)}^{-1}$), a small amount of rain ($1 \leq P < 10 \text{ mm (12 h)}^{-1}$), a moderate amount of rain ($10 \leq P < 25 \text{ mm (12 h)}^{-1}$), and a large amount of rain ($P \geq 25 \text{ mm (12 h)}^{-1}$).

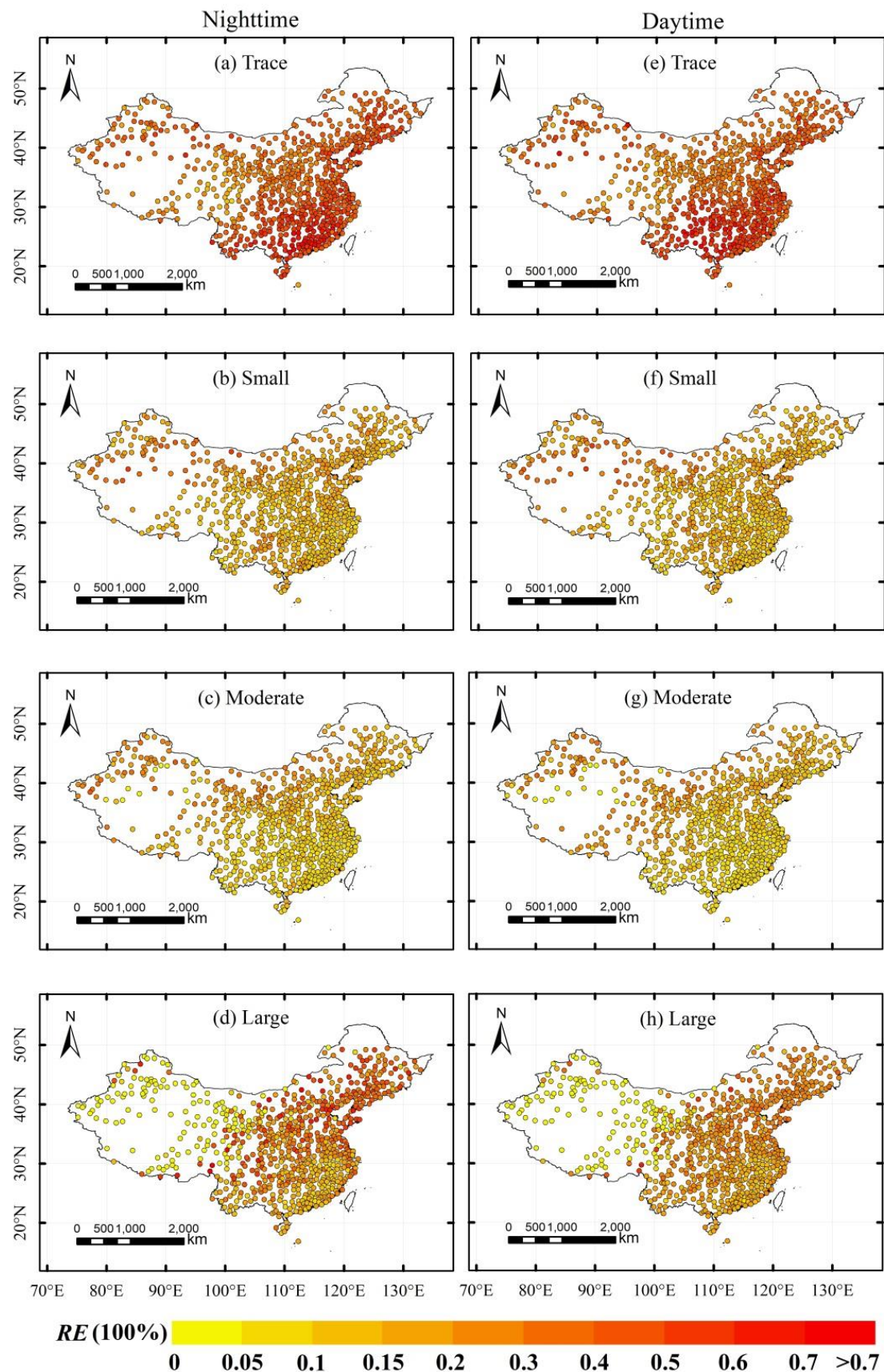


Figure 12. As in Figure 11, but for the intensity of precipitation.

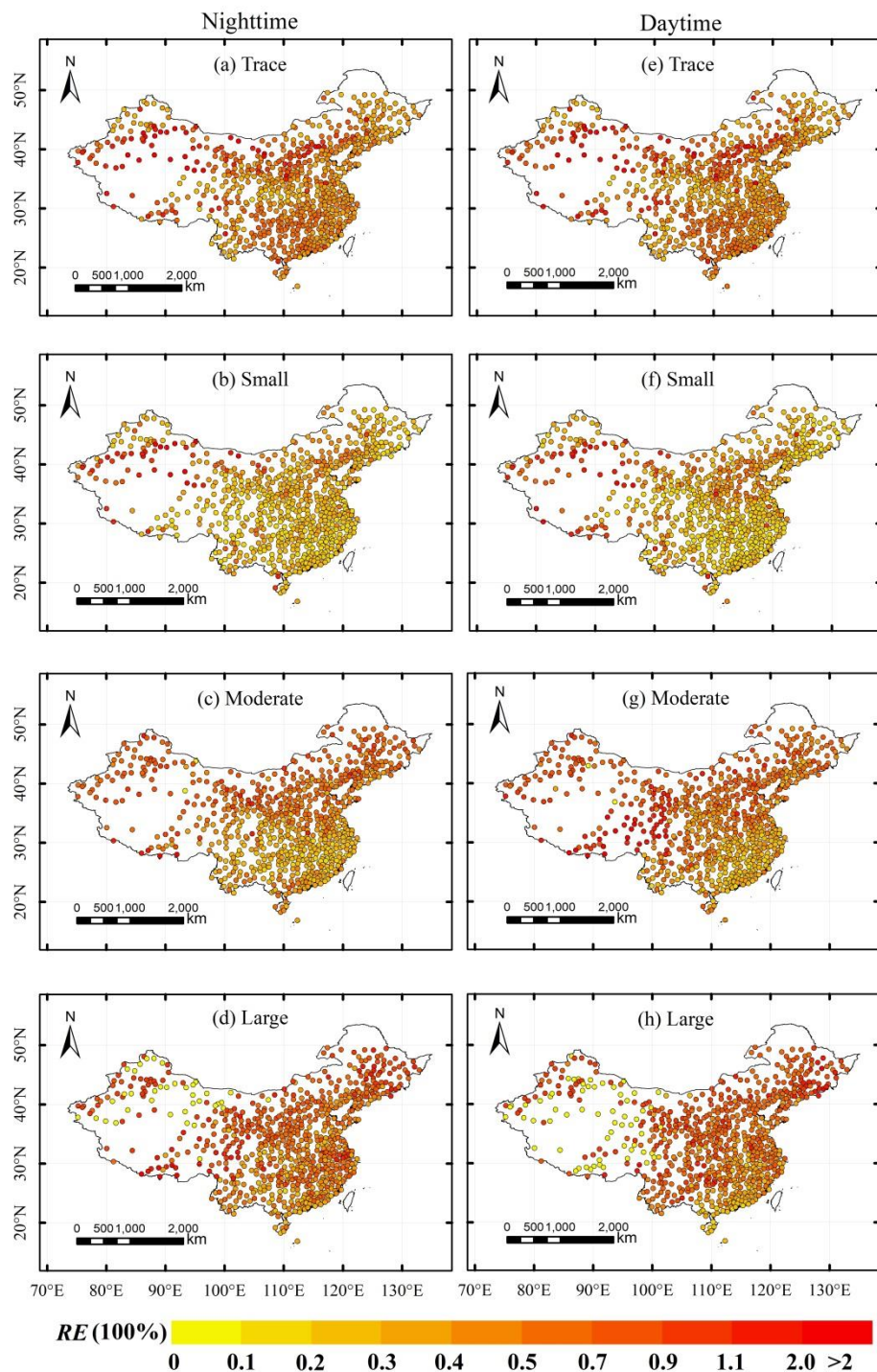


Figure 13. As in Figure 11, but for the amount of precipitation.

5. Discussion

5.1. Uncertainties in Estimates of Trace Amounts of Rain

In general, the TRMM 3B42V7 indicated good agreement with the data observed at the stations (except for trace amounts of rain) for the frequency and amount of precipitation. This is consistent with the findings of previous studies [58]. The frequency of precipitation as a trace amount of rain detected by the satellite was significantly smaller than that observed at the stations, with a trend of decrease. To the best of our knowledge, the ability of the satellite to capture trace precipitation was inadequate,

and research has shown that the TRMM 3B42 underestimated the frequency of low-intensity rainfall events [61].

However, note that the trend of the frequency of precipitation as a trace amount of rain was decreasing (Figure 2a₁,b₁) with statistical significance. Combined with Figure 8, we see that the precipitation was underestimated in south and northeast China. The frequency of a small amount of rain has significantly decreased in south China over the past 50 years [62,63]. However, the satellite data magnified this trend of reduction.

5.2. Negative Correlation between Frequency and Intensity

For both interannual variation and the seasonal cycle, the precipitation amount from the 3B42 and that from station observations had a higher correlation and lower relative bias compared with the frequency and intensity of precipitation. This was because 3B42 products had already correctly used the GPCC gauge analyses to enhance the calibration. Moreover, Figures 2, 3, 5 and 6 indicated that the frequency and intensity of the TRMM 3B42 had a negative correlation (-0.89 for nighttime and -0.85 for daytime). As the precipitation amount was affected by both the frequency and intensity of precipitation, there was a trade-off between them, resulting in a better performance in recording the amount of precipitation [9].

Therefore, the satellite data could reproduce the interannual variation in the characteristics of daytime and nighttime amount of precipitation except in the case of a trace amount of rain, and could capture the reductions in small amounts of precipitation. The combined comparison of the frequency, intensity, and amount of precipitation showed that the amount may be more susceptible to frequency, and less affected by the intensity of precipitation. This was consistent with the conclusion that the precipitation amount may be dominated by its frequency [58,64–66].

5.3. Poor Performance Areas

The relative bias between the satellite data and the data obtained at the stations in east China was restricted to within 50%, but exceeded 200% in the northwest and the Tibetan Plateau. In general, satellite products perform poorly in arid and semiarid areas [67], as well as mountainous areas [68,69]. Our results confirmed that 3B42 products perform poorly over high-altitude zones and complex terrains, such as the Loess Plateau, the Tarim Basin, the Tian Shan Mountains, and the Tibetan Plateau.

This issue was more pronounced for trace amounts of rain in the northwestern regions and large amounts of rain in the Tibetan Plateau. One explanation was that raindrops evaporate before reaching the ground, but the satellite calculates precipitation from the scattering of ice crystals in the clouds [70]. For the Tibetan Plateau, the overestimation can be attributed to several factors. On the one hand, emissivity signals from lower surface temperatures at high altitudes may be misidentified as rainfall [71], as is the case on snowy or icy ground. On the other hand, the complex terrain and associated warm rain in the south of the Tibetan Plateau could also have caused significant bias in satellite rainfall estimates [72]. Additionally, the poor performance may also be attributed to the sparse ground gauge-based information adopted in the GPCC data for the bias adjustments. The relatively sparse stations in these two areas lead to the large bias. Therefore, satellite precipitation products still face a great challenge in accurately estimating the precipitation over high-altitude regions and desert areas [67].

The spatial patterns of performance in northwest China are also affected by the main type of precipitation actually observed, since different precipitating processes have different effects on atmospheric circulation and in turn affect precipitation differently. Therefore, identifying the dominated precipitation type can help to reveal the underlying reasons of the spatial patterns. It was reported that the potential increase in convective extreme events may be caused by the significantly increasing temperature in northwest China [73]. Previous studies also found that the increase of the heavy precipitation in summer is convective-dominated, while the decrease in autumn is stratiform-dominated [74]. Further research is needed to investigate the changes in convective

and stratiform precipitations and will be beneficial to meteorological research. Moreover, the error characteristics of satellite precipitation estimates can be further investigated in detail over different climatic regions [61]. Despite these limitations, our results showed the performance of 3B42 products under different categories of intensity of precipitation. This can also provide useful insights into errors in their calculations of the frequency and intensity of precipitation. Future studies need to focus on improving satellite data retrieval algorithms suitable for different intensities and properties of precipitation.

6. Conclusions

This study examined the ability of TRMM 3B42V7 precipitation products to reproduce the frequency, intensity, and amount of precipitation from 1998 to 2017. The calculations, including for interannual trends, seasonal cycle, and spatial distribution, were conducted using data from 747 meteorological stations as a benchmark. The conclusions can be summarized as follows:

- 1) TRMM 3B42 products can successfully reproduce interannual trends of the frequency and amount of precipitation, with an averaged correlation coefficient of 0.84 over the past two decades, except for trace amounts of rain. The TRMM data and gauge data had the strongest correlation for moderate and large amounts of rain ($CC > 0.9$), a moderate correlation for small amounts of rain, and the weakest correlation for trace amounts of rain.
- 2) Satellite products can effectively represent the seasonal shape of the frequency and amount of precipitation during the nighttime and daytime ($CC > 0.88$). However, there are deficiencies in the estimated intensity of precipitation, especially for trace and small amounts of rain. The TRMM 3B42 tended to overestimate the precipitation frequency in rainy months (May–August) but underestimate it in rainless months (October–March). The precipitation intensity yielded results contrary to this. Therefore, the biases in the frequency and intensity of precipitation in different months offset one another, and there is improved performance in terms of the estimated amount of precipitation.
- 3) A spatial comparison showed that the TRMM 3B42 can effectively represent the distribution of the daily precipitation amount over most of the eastern regions of China, but did not perform well in the Tibetan Plateau and northwest China. Moreover, the satellite products tended to underestimate small precipitation amounts in south China and large precipitation amounts in north China, but overestimated small precipitation amounts in north China and large precipitation amounts in south China.

In summary, the TRMM 3B42 products performed well in terms of the precipitation amount, followed by the frequency, and worst in terms of the intensity. Furthermore, their performance in terms of estimating the precipitation frequency was more similar to that concerning the precipitation amount than the intensity. Owing to the highest relative bias being in the northwest regions and the Tibetan Plateau, we think that 3B42 products should be used with caution in these areas, especially when estimating trace or large amounts of rain.

Author Contributions: Y.L. collected the data and carried out the experiment. G.W. designed the study. Y.L. and G.W. wrote the manuscript with support from B.G., K.W., and C.S. All authors discussed the results and contributed to the final manuscript. All authors have read and agreed to the published version of the manuscript.

Funding: This research was funded by the National Key R&D Program of China (2017YFA0603601), the National Natural Science Foundation of China (91647202, 41705086 and 41405098), and the Fundamental Research Funds for the Central Universities.

Acknowledgments: The authors thank the editor and the anonymous reviewers for their very helpful and insightful comments that led to a significant improvement of the quality of this manuscript. We also thank Ms. Fang Wang for her valuable comments on the evaluation statistics. The TRMM data used in this study were from the National Aeronautics and Space Administration (NASA; https://disc.gsfc.nasa.gov/datasets/TRMM_3B42_7/summary). The subdaily precipitation data were obtained from the China Meteorological Administration (CMA; <http://data.cma.cn/en/>).

Conflicts of Interest: The authors declare that they have no conflict of interest.

References

1. Dai, A.; Lin, X.; Hsu, K.-L. The frequency, intensity, and diurnal cycle of precipitation in surface and satellite observations over low- and mid-latitudes. *Clim. Dyn.* **2007**, *29*, 727–744. [[CrossRef](#)]
2. Jia, S.; Zhu, W.; Lü, A.; Yan, T. A statistical spatial downscaling algorithm of TRMM precipitation based on NDVI and DEM in the Qaidam Basin of China. *Remote Sens. Environ.* **2011**, *115*, 3069–3079. [[CrossRef](#)]
3. Baguis, P.; Roulin, E.; Willem, P.; Ntegeka, V. Climate change scenarios for precipitation and potential evapotranspiration over central Belgium. *Theor. Appl. Climatol.* **2009**, *99*, 273–286. [[CrossRef](#)]
4. Tan, M.L.; Ibrahim, A.L.; Yusop, Z.; Chua, V.P.; Chan, N.W. Climate change impacts under CMIP5 RCP scenarios on water resources of the Kelantan River Basin, Malaysia. *Atmos. Res.* **2017**, *189*, 1–10. [[CrossRef](#)]
5. Tan, M.; Duan, Z. Assessment of GPM and TRMM Precipitation products over Singapore. *Remote Sens.* **2017**, *9*, 720. [[CrossRef](#)]
6. Li, C.; Wang, R. Recent changes of precipitation in Gansu, Northwest China: An index-based analysis. *Theor. Appl. Climatol.* **2016**, *129*, 397–412. [[CrossRef](#)]
7. Mei, Y.; Anagnostou, E.N.; Nikolopoulos, E.I.; Borga, M. Error analysis of satellite precipitation products in mountainous basins. *J. Hydrometeorol.* **2014**, *15*, 1778–1793. [[CrossRef](#)]
8. Haile, A.T.; Yan, F.; Habib, E. Accuracy of the CMORPH satellite-rainfall product over Lake Tana Basin in Eastern Africa. *Atmos. Res.* **2015**, *163*, 177–187. [[CrossRef](#)]
9. Li, R.Z.; Wang, K.; Qi, D. Validating the integrated multisatellite retrievals for global precipitation measurement in terms of diurnal variability with hourly gauge observations collected at 50,000 stations in China. *J. Geophys. Res. Atmos.* **2018**, *123*, 10423–10442. [[CrossRef](#)]
10. Xu, F.; Guo, B.; Ye, B.; Ye, Q.; Chen, H.; Ju, X.; Guo, J.; Wang, Z. Systematical evaluation of GPM IMERG and TRMM 3B42V7 precipitation products in the Huang-Huai-Hai Plain, China. *Remote Sens.* **2019**, *11*, 697. [[CrossRef](#)]
11. Tang, G.; Ma, Y.; Long, D.; Zhong, L.; Hong, Y. Evaluation of GPM Day-1 IMERG and TMPA Version-7 legacy products over Mainland China at multiple spatiotemporal scales. *J. Hydrol.* **2016**, *533*, 152–167. [[CrossRef](#)]
12. Einfalt, T.; Arnbjerg-Nielsen, K.; Golz, C.; Jensen, N.-E.; Quirmbach, M.; Vaes, G.; Vieux, B. Towards a roadmap for use of radar rainfall data in urban drainage. *J. Hydrol.* **2004**, *299*, 186–202. [[CrossRef](#)]
13. Schneebeli, M.; Dawes, N.; Lehning, M.; Berne, A. High-resolution vertical profiles of x-band polarimetric radar observables during snowfall in the swiss alps. *J. Appl. Meteorol. Climatol.* **2013**, *52*, 378–394. [[CrossRef](#)]
14. Li, X.-H.; Zhang, Q.; Xu, C.-Y. Suitability of the TRMM satellite rainfalls in driving a distributed hydrological model for water balance computations in Xinjiang catchment, Poyang lake basin. *J. Hydrol.* **2012**, *426*–427, 28–38. [[CrossRef](#)]
15. Du, L.; Tian, Q.; Yu, T.; Meng, Q.; Jancso, T.; Udvardy, P.; Huang, Y. A comprehensive drought monitoring method integrating MODIS and TRMM data. *Int. J. Appl. Earth Obs. Geoinf.* **2013**, *23*, 245–253. [[CrossRef](#)]
16. Kummerow, C.; Barnes, W.; Kozu, T.; Shiue, J.; Simpson, J. The Tropical Rainfall Measuring Mission (TRMM) sensor package. *J. Atmos. Ocean. Technol.* **1998**, *15*, 809–817. [[CrossRef](#)]
17. Huffman, G.J.; Bolvin, D.T.; Nelkin, E.J.; Wolff, D.B.; Adler, R.F.; Gu, G.; Hong, Y.; Bowman, K.P.; Stocker, E.F. The TRMM Multisatellite Precipitation Analysis (TMPA): Quasi-global, multiyear, combined-sensor precipitation estimates at fine scales. *J. Hydrometeorol.* **2007**, *8*, 38–55. [[CrossRef](#)]
18. JOYCE, R.J.; JANOWIAK, J.E.; ARKIN, P.A.; XIE, P. CMORPH: A Method that Produces Global Precipitation Estimates from Passive microwave and infrared data at high spatial and temporal resolution. *J. Hydrometeorol.* **2004**, *5*, 487–503. [[CrossRef](#)]
19. HSU, K.-L.; GAO, X.; SOROOSHIAN, S.; GUPTA, H.V. Precipitation estimation from remotely sensed information using artificial neural networks. *J. Appl. Meteorol. Climatol.* **1997**, *36*, 1176–1190. [[CrossRef](#)]
20. Hou, A.Y.; Kakar, R.K.; Neeck, S.; Azarbarzin, A.A.; Kummerow, C.D.; Kojima, M.; Oki, R.; Nakamura, K.; Iguchi, T. The global precipitation measurement mission. *Bull. Am. Meteorol. Soc.* **2014**, *95*, 701–722. [[CrossRef](#)]
21. Tan, M.L.; Ibrahim, A.L.; Duan, Z.; Cracknell, A.P.; Chaplot, V. Evaluation of six high-resolution satellite and ground-based precipitation products over Malaysia. *Remote Sens.* **2015**, *7*, 1504–1528. [[CrossRef](#)]

22. Tan, M.; Tan, K.; Chua, V.; Chan, N. Evaluation of TRMM product for monitoring drought in the Kelantan River Basin, Malaysia. *Water* **2017**, *9*, 57. [[CrossRef](#)]
23. Tan, M.L.; Santo, H. Comparison of GPM IMERG, TMPA 3B42 and PERSIANN-CDR satellite precipitation products over Malaysia. *Atmos. Res.* **2018**, *202*, 63–76. [[CrossRef](#)]
24. Li, J.; Hsu, K.-L.; AghaKouchak, A.; Sorooshian, S. Object-Based assessment of satellite precipitation products. *Remote Sens.* **2016**, *8*, 547. [[CrossRef](#)]
25. Varikoden, H.; Samah, A.A.; Babu, C.A. Spatial and temporal characteristics of rain intensity in the peninsular Malaysia using TRMM rain rate. *J. Hydrol.* **2010**, *387*, 312–319. [[CrossRef](#)]
26. Pombo, S.; de Oliveira, R.P. Evaluation of extreme precipitation estimates from TRMM in Angola. *J. Hydrol.* **2015**, *523*, 663–679. [[CrossRef](#)]
27. Nastos, P.T.; Kapsomenakis, J.; Philandras, K.M. Evaluation of the TRMM 3B43 gridded precipitation estimates over Greece. *Atmos. Res.* **2016**, *169*, 497–514. [[CrossRef](#)]
28. Su, F.; Hong, Y.; Lettenmaier, D.P. Evaluation of TRMM Multisatellite Precipitation Analysis (TMPA) and Its Utility in Hydrologic Prediction in the La Plata Basin. *J. Hydrometeorol.* **2008**, *9*, 622–640. [[CrossRef](#)]
29. Michot, V.; Vila, D.; Arvor, D.; Corpelli, T.; Ronchail, J.; Funatsu, B.; Dubreuil, V. Performance of TRMM TMPA 3B42 V7 in replicating daily rainfall and regional rainfall regimes in the Amazon Basin (1998–2013). *Remote Sens.* **2018**, *10*, 1879. [[CrossRef](#)]
30. Almazroui, M. Calibration of TRMM rainfall climatology over Saudi Arabia during 1998–2009. *Atmos. Res.* **2011**, *99*, 400–414. [[CrossRef](#)]
31. Tekeli, A.E.; Fouli, H. Evaluation of TRMM satellite-based precipitation indexes for flood forecasting over Riyadh City, Saudi Arabia. *J. Hydrol.* **2016**, *541*, 471–479. [[CrossRef](#)]
32. Brown, J.E.M. An analysis of the performance of hybrid infrared and microwave satellite precipitation algorithms over India and adjacent regions. *Remote Sens. Environ.* **2006**, *101*, 63–81. [[CrossRef](#)]
33. Javanmard, S.; Yatagai, A.; Nodzu, M.I.; BodaghJamali, J.; Kawamoto, H. Comparing high-resolution gridded precipitation data with satellite rainfall estimates of TRMM_3B42 over Iran. *Adv. Geosci.* **2010**, *25*, 119–125. [[CrossRef](#)]
34. Chen, S.; Hong, Y.; Cao, Q.; Gourley, J.J.; Kirstetter, P.-E.; Yong, B.; Tian, Y.; Zhang, Z.; Shen, Y.; Hu, J.; et al. Similarity and difference of the two successive V6 and V7 TRMM multisatellite precipitation analysis performance over China. *J. Geophys. Res. Atmos.* **2013**, *118*, 13060–13074. [[CrossRef](#)]
35. Huang, Y.; Chen, S.; Cao, Q.; Hong, Y.; Wu, B.; Huang, M.; Qiao, L.; Zhang, Z.; Li, Z.; Li, W.; et al. Evaluation of version-7 TRMM multi-satellite precipitation analysis product during the beijing extreme heavy rainfall event of 21 July 2012. *Water* **2013**, *6*, 32–44. [[CrossRef](#)]
36. Zhao, T.; Yatagai, A. Evaluation of TRMM 3B42 product using a new gauge-based analysis of daily precipitation over China. *Int. J. Climatol.* **2014**, *34*, 2749–2762. [[CrossRef](#)]
37. Habib, E.; Henschke, A.; Adler, R.F. Evaluation of TMPA satellite-based research and real-time rainfall estimates during six tropical-related heavy rainfall events over Louisiana, USA. *Atmos. Res.* **2009**, *94*, 373–388. [[CrossRef](#)]
38. Chen, S.; Hong, Y.; Gourley, J.J.; Huffman, G.J.; Tian, Y.; Cao, Q.; Yong, B.; Kirstetter, P.-E.; Hu, J.; Hardy, J.; et al. Evaluation of the successive V6 and V7 TRMM multisatellite precipitation analysis over the Continental United States. *Water Resour. Res.* **2013**, *49*, 8174–8186. [[CrossRef](#)]
39. Qiao, L.; Hong, Y.; Chen, S.; Zou, C.B.; Gourley, J.J.; Yong, B. Performance assessment of the successive Version 6 and Version 7 TMPA products over the climate-transitional zone in the southern Great Plains, USA. *J. Hydrol.* **2014**, *513*, 446–456. [[CrossRef](#)]
40. Feidas, H. Validation of satellite rainfall products over Greece. *Theor. Appl. Climatol.* **2009**, *99*, 193–216. [[CrossRef](#)]
41. Melo, D.d.C.D.; Xavier, A.C.; Bianchi, T.; Oliveira, P.T.S.; Scanlon, B.R.; Lucas, M.C.; Wendland, E. Performance evaluation of rainfall estimates by TRMM multi-satellite precipitation analysis 3B42V6 and V7 over Brazil. *J. Geophys. Res. Atmos.* **2015**, *120*, 9426–9436. [[CrossRef](#)]
42. Wang, S.; Liu, J.; Wang, J.; Qiao, X.; Zhang, J. Evaluation of GPM IMERG V05B and TRMM 3B42V7 Precipitation products over high mountainous tributaries in Lhasa with dense rain gauges. *Remote Sens.* **2019**, *11*, 80. [[CrossRef](#)]
43. Yu, R.; Zhou, T.; Xiong, A.; Zhu, Y.; Li, J. Diurnal variations of summer precipitation over contiguous China. *Geophys. Res. Lett.* **2007**, *34*. [[CrossRef](#)]

44. Yu, R.; Xu, Y.; Zhou, T.; Li, J. Relation between rainfall duration and diurnal variation in the warm season precipitation over central eastern China. *Geophys. Res. Lett.* **2007**, *34*. [[CrossRef](#)]
45. Hirose, M. Spatial and diurnal variation of precipitation systems over Asia observed by the TRMM Precipitation Radar. *J. Geophys. Res. Atmos.* **2005**, *110*. [[CrossRef](#)]
46. KUMMEROW, C.; SIMPSON, J.; THIELE, O.; BARNES, W.; CHANG, A.T.C.; STOCKER, E.; ADLER, R.F.; HOU, A.; KAKAR, R.; WENTZ, F.; et al. The status of the Tropical Rainfall Measuring Mission (TRMM) after two years in orbit. *J. Appl. Meteorol. Climatol.* **2000**, *39*, 1965–1982. [[CrossRef](#)]
47. Simpson, J.; Kummerow, C.; Tao, W.-K.; Adler, R.F. On the Tropical Rainfall Measuring Mission (TRMM). *Meteorol. Atmos. Phys.* **1996**, *60*, 19–36. [[CrossRef](#)]
48. Liu, Z. Comparison of versions 6 and 7 3-hourly TRMM multi-satellite precipitation analysis (TMPA) research products. *Atmos. Res.* **2015**, *163*, 91–101. [[CrossRef](#)]
49. Prakash, S.; Mitra, A.K.; Momin, I.M.; Pai, D.S.; Rajagopal, E.N.; Basu, S. Comparison of TMPA-3B42 versions 6 and 7 precipitation products with gauge-based data over India for the southwest monsoon period. *J. Hydrometeorol.* **2015**, *16*, 346–362. [[CrossRef](#)]
50. Yong, B.; Chen, B.; Gourley, J.J.; Ren, L.; Hong, Y.; Chen, X.; Wang, W.; Chen, S.; Gong, L. Intercomparison of the Version-6 and Version-7 TMPA precipitation products over high and low latitudes basins with independent gauge networks: Is the newer version better in both real-time and post-real-time analysis for water resources and hydrologic extremes? *J. Hydrol.* **2014**, *508*, 77–87. [[CrossRef](#)]
51. Iguchi, T.; Kozu, T.; Kwiatkowski, J.; Meneghini, R.; Awaka, J.; Okamoto, K.i. Uncertainties in the rain profiling algorithm for the TRMM precipitation radar. *J. Meteorol. Soc. Japan* **2009**, *87A*, 1–30. [[CrossRef](#)]
52. Dinku, T.; Anagnostou, E.N. TRMM calibration of SSM/I algorithm for overland rainfall estimation. *Am. Meteorol. Soc.* **2006**, *45*, 875–886. [[CrossRef](#)]
53. Chen, F.; Gao, Y. Evaluation of precipitation trends from high-resolution satellite precipitation products over Mainland China. *Clim. Dyn.* **2018**, *51*, 3311–3331. [[CrossRef](#)]
54. Li, Z.; Yang, D.; Hong, Y. Multi-scale evaluation of high-resolution multi-sensor blended global precipitation products over the Yangtze River. *J. Hydrol.* **2013**, *500*, 157–169. [[CrossRef](#)]
55. Dai, A. Precipitation characteristics in eighteen coupled climate models. *J. Clim.* **2006**, *19*, 4605–4630. [[CrossRef](#)]
56. Ma, S.M.; Zhou, T.J.; Dai, A.G.; Han, Z.Y. Observed changes in the distributions of daily precipitation frequency and amount over China from 1960 to 2013. *J. Clim.* **2015**, *28*, 6960–6978. [[CrossRef](#)]
57. Huang, D.-Q.; Zhu, J.; Zhang, Y.-C.; Huang, Y.; Kuang, X.-Y. Assessment of summer monsoon precipitation derived from five reanalysis datasets over East Asia. *Q. J. R. Meteorol. Soc.* **2016**, *142*, 108–119. [[CrossRef](#)]
58. Zhou, C.; Wang, K. Contrasting Daytime and Nighttime Precipitation Variability between Observations and Eight Reanalysis Products from 1979 to 2014 in China. *J. Clim.* **2017**, *30*, 6443–6464. [[CrossRef](#)]
59. Jiang, L.; Bauer-Gottwein, P. How do GPM IMERG precipitation estimates perform as hydrological model forcing? Evaluation for 300 catchments across Mainland China. *J. Hydrol.* **2019**, *572*, 486–500. [[CrossRef](#)]
60. Xu, R.; Tian, F.; Yang, L.; Hu, H.; Lu, H.; Hou, A. Ground validation of GPM IMERG and TRMM 3B42V7 rainfall products over southern Tibetan Plateau based on a high-density rain gauge network. *J. Geophys. Res. Atmos.* **2017**, *122*, 910–924. [[CrossRef](#)]
61. Qin, Y.; Chen, Z.; Shen, Y.; Zhang, S.; Shi, R. Evaluation of satellite rainfall estimates over the Chinese Mainland. *Remote Sens.* **2014**, *6*, 11649–11672. [[CrossRef](#)]
62. Qian, Y.; Gong, D.; Fan, J.; Leung, L.R.; Bennartz, R.; Chen, D.; Wang, W. Heavy pollution suppresses light rain in China: Observations and modeling. *J. Geophys. Res. Atmos.* **2009**, *114*. [[CrossRef](#)]
63. Fu, C.; Dan, L. Trends in the different grades of precipitation over South China during 1960–2010 and the possible link with anthropogenic aerosols. *Adv. Atmos. Sci.* **2014**, *31*, 480–491. [[CrossRef](#)]
64. Trenberth, K.E.; Dai, A.; RASMUSSEN, R.M.; PARSONS, D.B. The changing character of precipitation. *Bull. Am. Meteorol. Soc.* **2003**, *84*, 1205–1218. [[CrossRef](#)]
65. OKI, T.; MUSIAKE, K. Seasonal change of the diurnal cycle of precipitation over Japan and Malaysia. *J. Appl. Meteorol.* **1994**, *33*, 1445–1463. [[CrossRef](#)]
66. Trenberth, K.E.; Zhang, Y. How often does it really rain? *Bull. Am. Meteorol. Soc.* **2018**, *99*, 289–298. [[CrossRef](#)]
67. Huang, A.; Zhao, Y.; Zhou, Y.; Yang, B.; Zhang, L.; Dong, X.; Fang, D.; Wu, Y. Evaluation of multisatellite precipitation products by use of ground-based data over China. *J. Geophys. Res. Atmos.* **2016**, *121*, 654–675. [[CrossRef](#)]

68. Dinku, T.; Chidzambwa, S.; Ceccato, P.; Connor, S.J.; Ropelewski, C.F. Validation of high-resolution satellite rainfall products over complex terrain. *Int. J. Remote Sens.* **2008**, *29*, 4097–4110. [[CrossRef](#)]
69. Maggioni, V.; Meyers, P.C.; Robinson, M.D. A Review of merged high-resolution satellite precipitation product accuracy during the tropical Rainfall Measuring Mission (TRMM) era. *J. Hydrometeorol.* **2016**, *17*, 1101–1117. [[CrossRef](#)]
70. MCCOLLUM, J.R.; GRUBER, A.; BA, M.B. Discrepancy between Gauges and Satellite Estimates of Rainfall in Equatorial Africa. *J. Appl. Meteorol.* **2000**, *39*, 666–679. [[CrossRef](#)]
71. Nasrollahi, N.; Hsu, K.; Sorooshian, S. An artificial neural network model to reduce false alarms in satellite precipitation products using MODIS and CloudSat observations. *J. Hydrometeorol.* **2013**, *14*, 1872–1883. [[CrossRef](#)]
72. Shige, S.; Kida, S.; Ashiwake, H.; Kubota, T.; Aonashi, K. Improvement of TMI rain retrievals in mountainous areas. *J. Appl. Meteorol. Climatol.* **2013**, *52*, 242–254. [[CrossRef](#)]
73. Li, B.F.; Chen, Y.N.; Shi, X. Why does the temperature rise faster in the arid region of northwest China? *J. Geophys. Res. Atmos.* **2012**, *117*. [[CrossRef](#)]
74. Han, X.; Xue, H.; Zhao, C.; Lu, D. The roles of convective and stratiform precipitation in the observed precipitation trends in Northwest China during 1961–2000. *Atmos. Res.* **2016**, *169*, 139–146. [[CrossRef](#)]



© 2020 by the authors. Licensee MDPI, Basel, Switzerland. This article is an open access article distributed under the terms and conditions of the Creative Commons Attribution (CC BY) license (<http://creativecommons.org/licenses/by/4.0/>).